RESEARCH

One-step Preparation of Silicate Coatings on AZ91D Magnesium Alloy Surface for Boosting its Corrosion Resistance

Min Jiang[1] · Jianmao Wu[1] · Jiyuan Zhu[1]

Abstract

The silicate composite coating with corrosion resistance was prepared by one-step hydrothermal method on the surface of magnesium alloys. The effect of different time and temperature on the corrosion resistance of silicate coatings was also investigated. Electrochemical tests were carried out on AZ91D and coated samples in 3.5 wt% NaCl solution. The microscopic morphology and composition of the coated samples as well as the anti-corrosion mechanism were investigated through the tests. The results showed that the cluster structure on the surface of the coating effectively prevented the electrolyte from entering the surface of the magnesium alloy, and the corrosion current of the coating decreased by four orders of magnitude compared with that of the magnesium alloy substrate, which greatly improved the corrosion resistance of the magnesium alloy. This provides a new approach to inorganic clay in metal corrosion prevention.

Keywords Magnesium · Hydrothermal method · Anti-corrosion · Silicate coatings

1 Introduction

Magnesium and its alloys provide excellent electromagnetic shielding, strong damping qualities, high thermal conductivity, superior machinability, and ease of recycling [1, 2]. They also exhibit a good strength-to-weight ratio. Due to these characteristics, it is widely used in a variety of industries, including computer and automobile components, aerospace components, and biomedicine. Magnesium alloys are also used as implant materials in the biomedical area due to their inherent biodegradability and antibacterial properties in the physiological environment [3–6]. However, the extensive application of magnesium alloys has been hampered by their strong chemical activity. Magnesium alloys are susceptible to galvanic corrosion, which leads to metal pitting and loss of mechanical stability. Magnesium alloys mostly experience hydrogen evolution reactions in aqueous solutions [7, 8]. The presence of pitting on the surface of magnesium alloys is an indication of widespread corrosion. The reaction of magnesium alloys in aqueous solutions results in surface damage and reduced protection [9]. Generating coatings on the surface of magnesium alloys is one of the effective ways to enhance the corrosion protection of magnesium alloys. The generated coating separates the environment and the metal, thus protecting the magnesium alloy [10].

A variety of methods such as spraying [11], PVD/CVD [12, 13], electrodeposition [14, 15], chemical conversion [16], electroplating/chemical plating [17, 18], and anodic oxidation [19, 20] have been employed to fabricate anti-corrosion coatings on magnesium alloy surfaces. Among these, the hydrothermal method has received a lot of attention for its advantages of simplicity, controllability, low cost, no pollution, and good protection. The substrate and coating material are enclosed in a hydrothermal container at a specific temperature, and the reaction time varies from a few minutes to several hours in the hydrothermal process. No specific equipment is required because the diffusion of atoms from the substrate and covering material induces a combination of them [21]. The crystalline form of the hydrothermally reacted particles allows for better control of their size and shape, although the reaction time is a little longer compared to vapor phase deposition [22].

Because they are nontoxic and environmentally friendly, silicate coatings are widely used in applications of corrosion protection [23]. Montmorillonite (MMT)

✉ Jiyuan Zhu
zhujiyuanscut@163.com

1 Key Laboratory of Advanced Manufacturing
and Automation Technology, Guilin University
of Technology), Education Department of Guangxi Zhuang
Autonomous Region, Guilin 541006, China

is the primary component of layered silicate bentonite, an inorganic layered clay with the chemical formula $Al_2\text{-}xMg_x(Si_4O_{10})(OH)_2\text{-}(Na_x\text{-}nH_2O)$. Due to its widespread distribution in the natural environment and low price, it is one of the clays that has been investigated extensively. Numerous physical characteristics of clay include granularity, hardness, high flexibility, binding ability, and proper contractibility. Although they are frequently used in corrosion protection due to their small particle size and high surface area due to their complex porous structure, their hydrophilic nature and surface flaws also restrict their long-term development in corrosion protection [24]. Zhang et al. [25] prepared an epoxy coating of polyaniline/organomontmorillonite (PANI/OMMT) powder on the surface of AZ91D magnesium alloy, which still had high corrosion protection properties after immersion experiments. Zamanizadeh et al. [26] coated stainless steel surfaces by adding montmorillonite to emulsified bitumen in water and showed that clay nanolayer additions improved the corrosion resistance of the coatings. All the above experiments have demonstrated that montmorillonite can be used as a corrosion inhibitor to improve the corrosion resistance of metal surfaces, but their drawbacks are also obvious in such aspects as the complicated experimental steps, long consumption time, and use of some toxic materials, which is not conducive to a green and wide application.

In this paper, a non-polluting method for preparing coatings on the surface of magnesium alloys was proposed, which has the advantages of non-toxic materials, a simple process, short consumption time, and good corrosion protection, and the corrosion current density of the samples is reduced by four orders of magnitude compared with AZ91D. The corrosion effect in NaCl solution was investigated and the formation and anti-corrosion behavior of the coating were discussed.

2 Experimental

2.1 Materials

AZ91D of $20 \times 20 \times 5$ mm^3 was used as the base material for the experiments, and its alloy composition is shown in Table 1. The chemical reagents used in the experiments were ethanol (AR) purchased from Tianjin Fuyu Fine Chemical Co. Montmorillonite was purchased from ShanlinShiyu Mineral Products Co. Sodium hydroxide (AR) purchased from Xilong Science Co. Silica was purchased from Rhawn Reagent.

2.2 Preparation

The substrate is sanded with SiC sandpaper of 500#, 1000#, 1500#, and 2000#, then ultrasonically cleaned in deionized water and anhydrous ethanol to remove residues from the magnesium alloy surface and dried naturally. After measuring 65 mL of deionized water, 0.44 g NaOH, 0.44 g silica, and 3.0 g montmorillonite were added and agitated magnetically until fully dissolved. The reactor was then completely sealed before being placed in the oven. The schematic diagram for the experimental procedures is shown in Fig. 1. Temperature and time were the experiment's variables, and the reaction temperature ranged from 160 to 180 °C. The samples were taken out after 2–4 h, then the surfaces were cleaned of reaction reagents and dried at 60 °C for 2 h. Samples produced at different times and temperatures were named as ms-160-3, ms-170-2, ms-170-3, ms-170-4, ms-180-3.
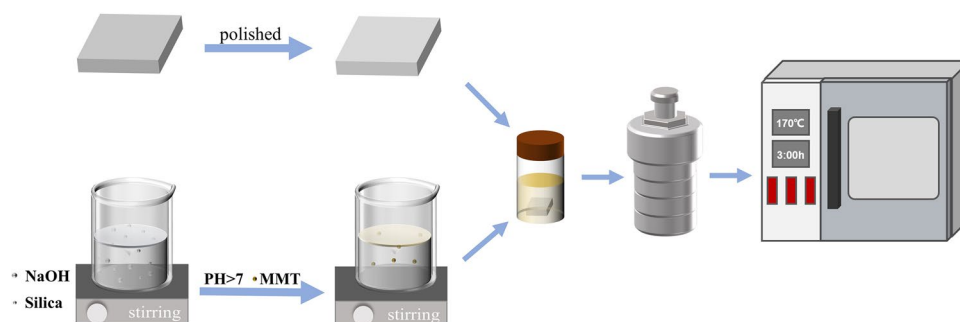
2.3 Surface Characterizations

The surface structure and cross-sectional morphology of the composite coatings were characterized by SEM (SEM, KYKY-EM6900, KYKY, Beijing, China). The surface and

Table 1 Chemical compositions of AZ91D alloy (wt%)

Element	Al	Zn	Mn	Si	Fe	Mg
Wt.%	9.3	0.63	0.32	0.05	0.003	balance

Fig. 1 Schematic diagram for the experimental procedures

cross-sectional microscopic morphology obtained by SEM provide a visual representation of the quality of the prepared samples. The crystal microstructure of the samples was analyzed by X-ray diffraction (XRD, D8 Advance, Bruker AXS, Karlsruhe, Germany). The chemical composition and elemental valence of the samples were measured and analyzed by X-ray photoelectron spectroscopy (XPS, Escalab 250Xi, Thermo Scientific, Waltham, America).

2.4 Electrochemical Measurements

The samples were tested electrochemically using a computer-controlled CS2350H electrochemical workstation (Wuhan Corrtest Instruments Corp, Ltd, Wuhan, China). Measurements were carried out at room temperature and the workstation used a conventional three-electrode measurement system with a platinum auxiliary electrode, an Ag/AgCl (saturated KCl) electrode as the reference electrode, and a test sample with a working area of 1 cm^2 as the working electrode. To ensure steady conditions, the sample was tested at open circuit potential for 30 min before the test. Polarization curves were obtained at a scan rate of 1 mV s^{-1}. The test potentials were set from -0.5 to 1 V. The operating frequency range was from 0.01 Hz to 100,000 Hz with an AC amplitude of 5 mV. The electrochemical test results were fitted to an equivalent circuit model and analyzed by the software.

2.5 Immersion Testing

To test the samples for long-term corrosion, immersion tests were carried out on the samples. Both the magnesium alloy substrate and the samples were carried out according to ASTM-G3172. Both were removed from a 5wt% NaCl solution every 24 h and subsequently immersed in a mixture of 20 wt% CrO$_3$ and 1 wt% AgNO$_3$ to remove corrosion products. Afterward, they were washed and dried with deionized water and the weight loss was recorded using an electronic balance while photographs were taken for surface analysis of the samples.

3 Result and Discussion

3.1 Characterization of Coating

3.1.1 Morphology of the Surface

The surface morphology of the coatings prepared at 170 °C was photographed. Figure 2a, b, c shows the surface morphology of the coatings at different reaction times. Scratches after polishing of the substrate are visible under the coatings, indicating that the coatings are thin and have protrusions,

cracks, and tiny particles dispersed on the surface. After local amplification, the surface structure of the coating ms-170-3 is shown in Fig. 2b, d, f. The protrusions on the coating surface are unevenly sized and irregularly shaped particles, and the degree of tightness of the particle bonding varies. In Fig. 2e, particles are tightly bound as clusters with small gaps, while the distance between particles in Fig. 2f differs considerably.
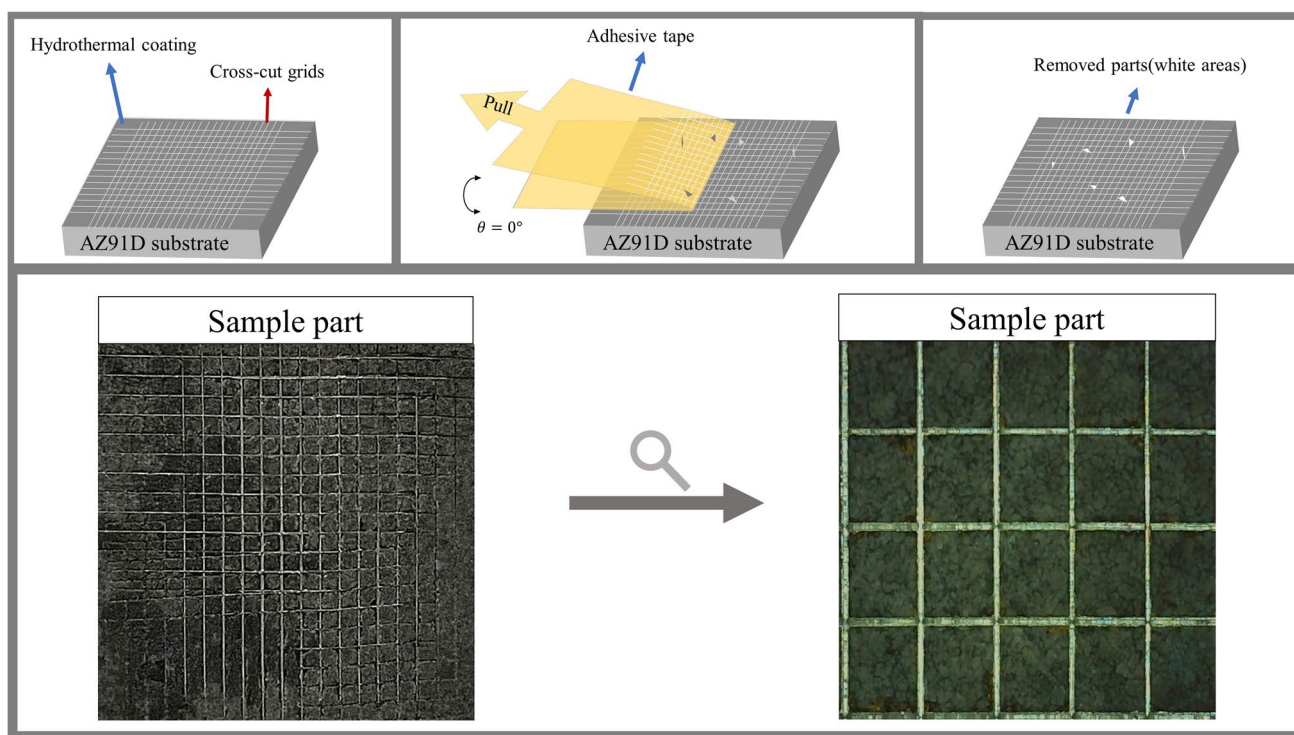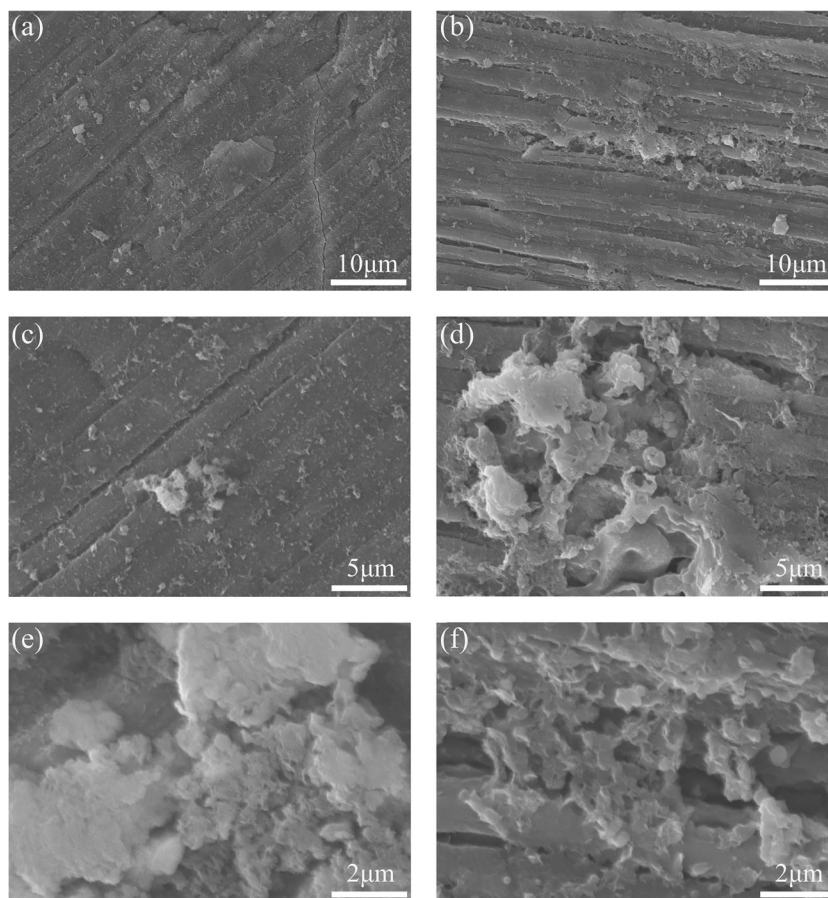
3.1.2 Cross-cut Tape Test

Surface roughness affects the adhesion between the coating and the substrate. The adhesion of the coating to the substrate resists the coating coming off the substrate, which is an important characteristic for obtaining the mechanical integrity of the coating system [27]. In addition, it has an important influence on the long-term stability of the coated implant. Figure 3 reveals the process of the test. The adhesion of the coating to the AZ91D magnesium alloy substrate was tested according to the American Society for Testing and Materials (ASTM-D3359). There were small flaking pieces at the intersection of the cut, with no more than 5% actual breakage within the scribed area, and the adhesion quality was 4B compared to the adhesion test standard, indicating a strong bond between the magnesium alloy substrate and the coating. Coatings generated in situ on the substrate surface by a chemical reaction between the solution and the magnesium alloy, unlike those deposited on the surface of magnesium alloys, generally exhibit stronger adhesion and mechanical stability than colloidal deposition [28].

3.2 XRD Analysis

The XRD pattern of the magnesium alloy with the sample is shown in Fig. 4. The narrower peak shape and higher strength of the magnesium alloy matrix indicate larger grains [29]. Diffraction peaks of Mg (PDF#01-079-6692) and Mg$_{17}$Al$_{12}$ (PDF#01-014-7592) are only present in the matrix. The XRD pattern of the sample shows diffraction peaks of Mg$_{17}$Al$_{12}$ with Mg still present, due to the penetrating nature of the XRD detection. A comparison of the XRD patterns of the matrix and the sample shows that the peaks of Mg and Mg$_{17}$Al$_{12}$ in the sample are reduced compared to the magnesium alloy matrix and converted into compounds. The compounds are Mg(OH)$_2$ (PDF#97-003-4401), which is converted by the reaction between OH$^-$ and magnesium alloy matrix under the presence of alkaline conditions, and Mg$_2$SiO$_4$ (PDF#01-070-2165), which is formed by the exchange of cations in the solution, and the diffraction peaks of the two compounds have lower heights and intensities, which indicate that the surface species contain substances with smaller grains, which is conducive to the formation of corrosion product film layers with protective effects. The
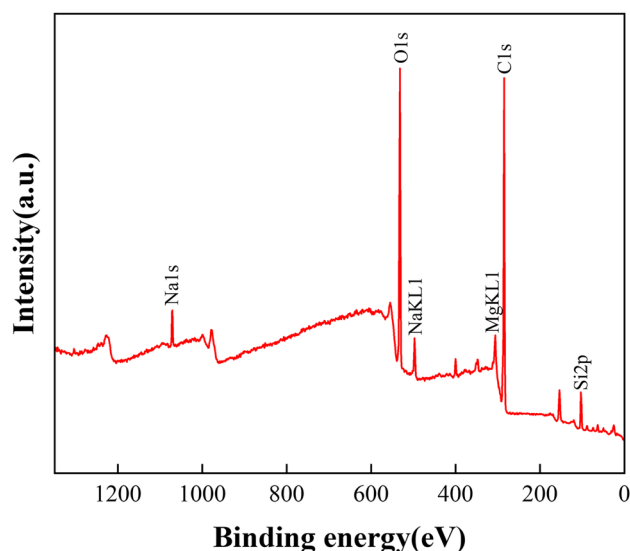
Fig. 2 SEM micrographs of the coating **a** ms-170-2, **b** ms-170-3, **c** ms-170-4, **d** ms-170-3, **e** ms-170-4, **f** ms-170-3

Fig. 3 Surface observation of cross-cut tape test on the sample
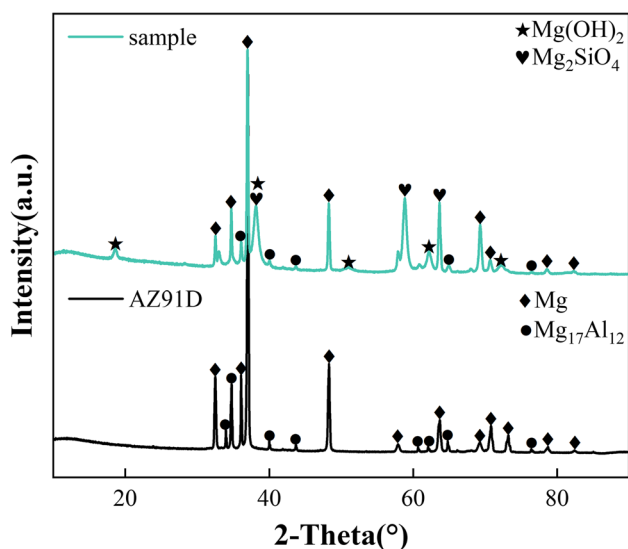
Fig. 4 The X-ray diffraction pattern of the substrate and the sample ms-170-3

Fig. 5 XPS survey of the sample

corrosion product film layer effectively slows down the corrosion rate of the magnesium alloy surface [30, 31].

3.3 XPS Chemical Characterization

X-ray photoelectron spectroscopy was performed on the surface of the magnesium alloy using XPS testing to analyze the composition of the material on the surface of the coating by the presence of characteristic elements and the internal electron arrangement. Figure 5 shows the full XPS survey of the coating, with the main elements of Na, O, C, Mg, and Si on the surface.

Figure 6a-f shows the high-resolution XPS spectra of C1s, O1s, Mg1s, Na1s, Si2p, and Al2p, respectively. In the C1s (Fig. 6a) narrow scan spectrum, there are three peaks at binding energies of 284.8 eV, 286.4 eV, and 288.06 eV, corresponding to carbon-carbon bonds (C-C), carbon-oxygen single bonds (C-O-C), carbon-oxygen double bonds (O-C=O). The narrow scan spectrum of O1s (Fig. 6b) decomposes into two peaks with binding energies of 531.2 eV corresponding to the hydroxide of magnesium and 530.3 eV corresponding to metal oxide [32, 33]. The characteristic peaks of Na1s (Fig. 6d) at a binding energy of 1071.2 eV and Al 2p (Fig. 6f) at a binding energy of 73.4 eV correspond to the dissolution of montmorillonite in alkaline solution and the hydrothermal reaction of sodium and aluminum ions [34]. The characteristic peak of Mg 1s (Fig. 6c) at 1303.1 eV is associated with metallic Mg [35]. Si has a variety of chemical states and is primarily a thin film composed of SiO_2 and SiO [36], Robin et al. [37] suggested that when used as passivation films, Si exists in the form of mixed silicates (SiO_4^{4-}). the peak value of Si 2p (Fig. 6e) at 101.8 eV is the same as the binding energy reported by Okada et al. [38]. From the analysis, it can be deduced that the surface composition of the sample is comprised of $Mg(OH)_2$ and silicate.

3.4 Potentiodynamic Polarization Curve

Figure 7 presents the potentiodynamic polarization curve for AZ91D and samples prepared at different reaction times and temperatures. The polarization curves provide valuable information about the corrosion current density (Icorr) and corrosion potential (Ecorr).

Table 2 shows the polarization parameters on corrosion potentials and corrosion currents measured by the Tafel extrapolation method. Corrosion current density reflects the corrosion sensitivity of the coating [39]. After a reaction time of 3 h or longer, the prepared samples displayed a significant decrease in I_{corr}, at least by three orders of magnitude. The samples at a temperature of 170 °C showed the lowest corrosion current density and corrosion rate, indicating improved corrosion resistance. Additionally, these samples showed a decrease in I_{corr} of four orders of magnitude compared to the AZ91D.

The bar diagram in Fig. 8 displays the data for corrosion current density and corrosion rate. It is evident that with the exception of the sample that reacted at 170 ℃ for 3 h, the corrosion current density of the samples was significantly lower (0.00426 μA/cm^2) than that of the magnesium alloy substrate (32.97 μA/cm^2). This suggests that the coating effectively prevents electrolyte penetration. However, the corrosion rate of the sample after 2 h of reaction was higher (45.76 μA/cm^2) than that of the magnesium alloy substrate. This could be attributed to insufficient reaction time, as the

Fig. 6 The XPS spectra of **a** C1s **b** O1s **c** Mg1s **d** Na1s **e** Si 2p **f** Al 2p
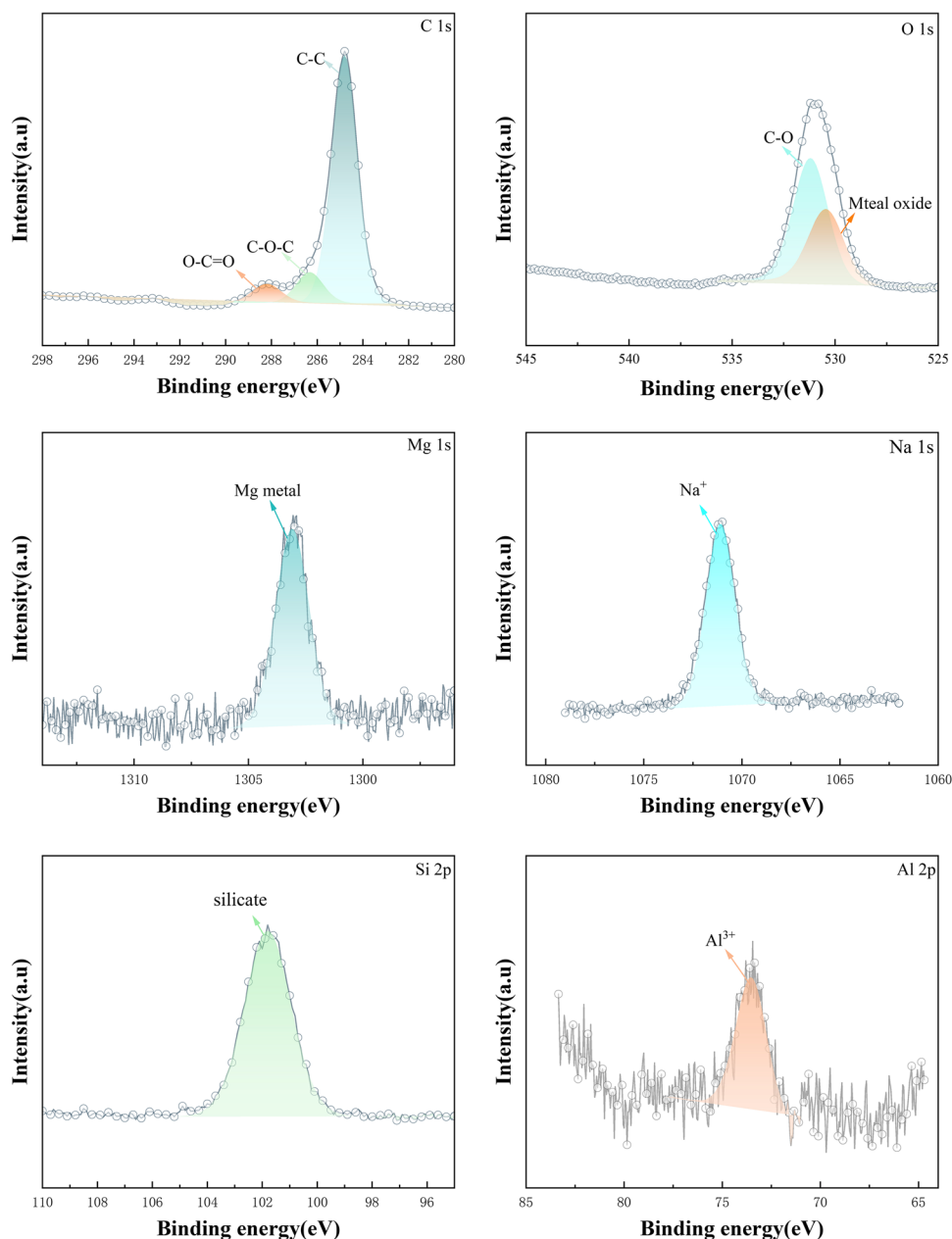

coating had not yet formed on the surface of the magnesium alloy in the strong alkaline environment, resulting in surface etching.

3.5 Electrochemical Impedance Spectroscopy Measurements

The EIS test analyzes the impedance of the system and creates equivalent circuits for magnesium alloy substrates and hydrothermally treated samples. The results demonstrate that the fitted curves closely match the findings of the EIS analysis. The Nyquist plot of the magnesium alloy reveals a capacitive circuit in the high and medium frequency ranges. The high-frequency capacitive loops may be attributed to the combination of interfacial capacitance and charge transfer resistance [28, 40, 41]. The Nyquist diagram represents the size of the capacitance loop, which directly indicates the corrosion resistance of the test sample. A larger diameter indicates better corrosion resistance [39]. In Fig. 9, the capacitance loop of the AZ91D substrate displays only one half cycle, and its diameter is much larger than that of the substrate. The Nyquist curves of the samples allow the observation of the presence of a second capacitance arc in the sample representing the double layer capacitance of the metal surface, close to the 45° slash, which may be due to the presence of Warburg impedance caused by the planar diffusion process [42].
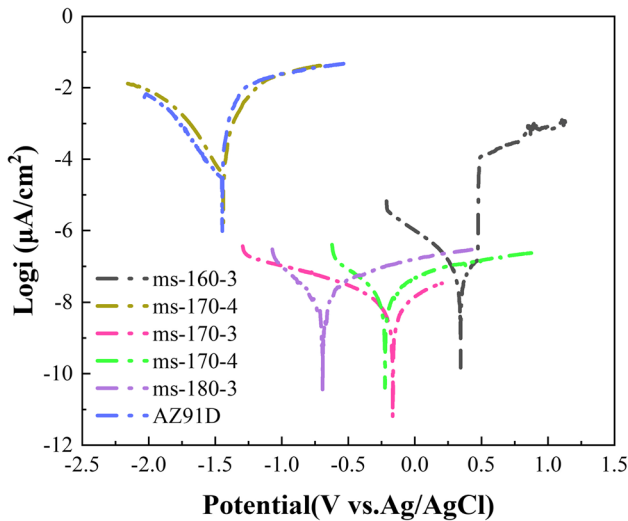
**Fig. 7** Polarization curves of different samples in 3.5 wt% NaCl solution

Table 2 The polarization corrosion parameters of the samples and AZ91D

| sample	$I_{corr}(\mu A/cm^2)$	$E_{corr}(V)$	Corrosion Rate(μm/y)
160℃-3 h	0.0592 ± 0.0003	0.29986	1.2549 ± 0.0006
170℃-2 h	45.755 ± 0.005	-1.4844	970.36 ± 0.004
170℃-3 h	0.00426 ± 0.00005	-0.20994	0.0904 ± 0.00004
170℃-4 h	0.0136 ± 0.00004	-0.2682	0.2882 ± 0.00002
180℃-3 h	0.0107 ± 0.00004	-0.73706	0.2268 ± 0.00004
AZ91D	32.973 ± 0.007	-1.4924	699.29 ± 0.002
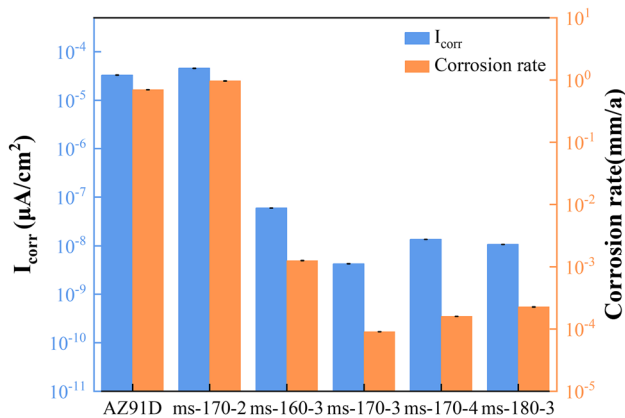
Fig. 8 I_{corr} and corrosion rate of different samples

In the Bode plot, a higher impedance modulus |Z| at lower frequencies indicates good corrosion resistance [43]. Figure 10 shows the impedance spectra of samples prepared at different times and temperatures. In the frequency range of 10^{-2}-10^3 Hz, the |Z| of the samples is 1–4 orders of
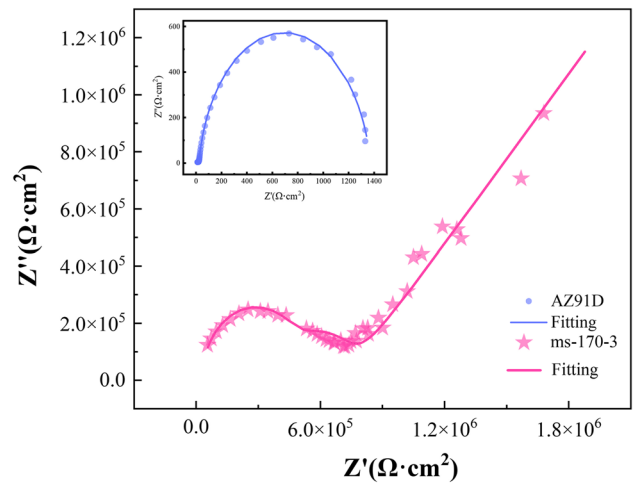
Fig. 9 The Nyquist plots
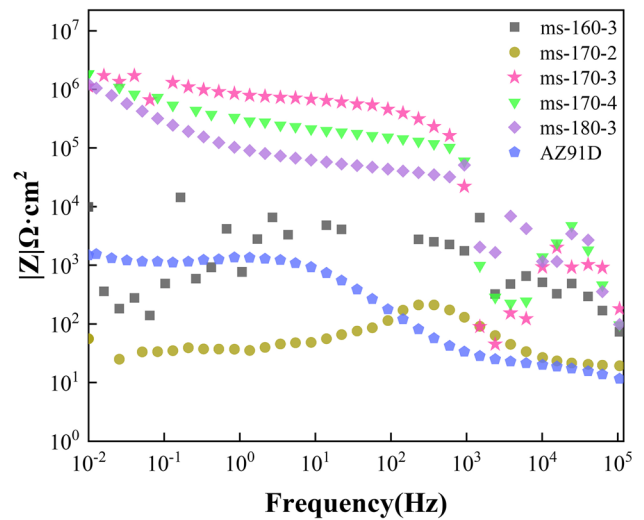
Fig. 10 The Bode plots

magnitude higher than that of the substrate, indicating that the prepared films are corrosion-resistant, and |Z| tends to become smaller with the increase of the frequency in the test, which is due to the corrosion caused by the coating of the magnesium alloy surface by the Cl$^-$ in solution [44]. The polarization curves are consistent with the electrochemical impedance spectra, which demonstrates the corrosion resistance of the coating on the magnesium alloy surface.

In Fig. 11, the circuit diagram illustrates the behavior of the magnesium alloy substrate. The resistance of the solution is denoted as Rs, the double-layer capacitance of the magnesium alloy is denoted as CPE1, and the charge transfer resistance is denoted as R_{ct}. In a NaCl solution, the dissolution of Mg occurs in the film-free region, and the resulting Mg^{2+} ions diffuse through the porous Mg(OH)$_2$ [45]. The corrosion process initiates with the formation of
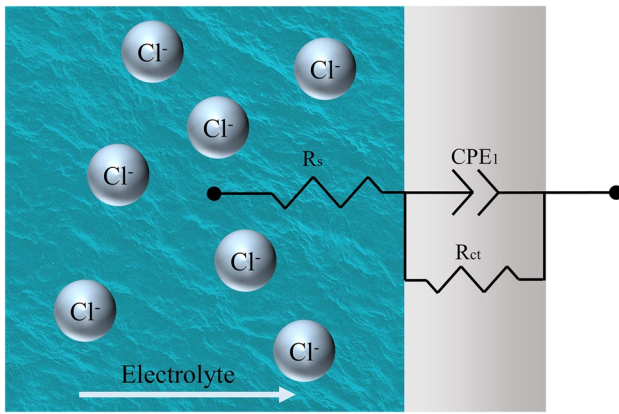
Fig. 11 The equivalent circuit of AZ91D.

a loose film of $Mg(OH)_2$ on the surface of the magnesium alloy, which acts as a protective barrier against electrolyte penetration. However, this film quickly decomposes and transforms into highly soluble $MgCl_2$ in the presence of chloride ions due to its solubility in water and weak structure. As a result, porous corrosion occurs, and the ability to effectively resist the electrolyte in the solution diminishes over time [46, 47].

The equivalent circuit for the hydrothermal coating is shown in Fig. 12. The components of the equivalent circuit correspond to the corrosion system [48], The electrolyte first penetrates the coating with anti-corrosion properties, which can effectively mitigate the penetration of the electrolyte in solution and thus anti-corrosion properties. CPE and R_{ct} denote the capacitance of the composite coating and the constant-phase original and resistive elements of the solution penetrating the coating, respectively [36]. The high-frequency circuit reflects the characteristics of the outer layer of the coating, due to the charge-transfer effect resulting from the double-layer capacitance of the film formed on the surface [49]. The equivalent circuit data were summarized in Table 3.
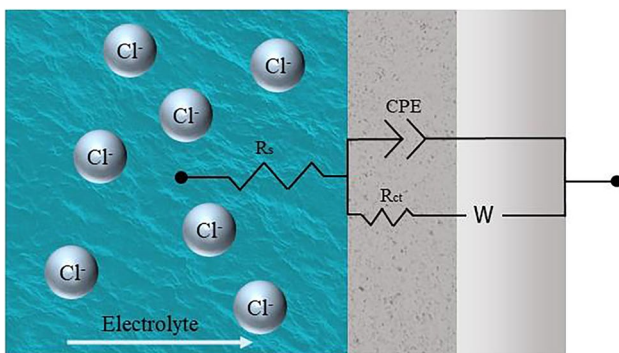

Fig. 12 The equivalent circuit of the coating

Table 3 Equivalent circuit data of AZ91D substrate and the sample

Sample	$R_s (\Omega/cm^2)$	$R_{ct} (\Omega/cm^2)$	CPE (F/cm^2)	$W (\Omega/cm^2)$
AZ91D	17.37	1.315×10^3	2.5914×10^{-5}	/
ms-170-3	1214	5.71×10^6	4.684×10^{-9}	3.2529×10^6

3.6 Immersion Test

To verify the long-term corrosion resistance of the coating, the ms-170-3 sample with the best corrosion resistance underwent a test where the magnesium alloy substrate was immersed in a 5 wt% NaCl solution for 168 h. Figure 13 presents the surface morphology of the magnesium alloy substrate and the sample at 24-hour intervals. Over time, the number and density of pitting holes on the surface of the magnesium alloy substrate increased after immersion in the solution. Additionally, as the immersion time increased, the metal layer on the magnesium alloy surface gradually peeled off, exposing the corroded substrate. In contrast, the prepared samples with coating coverage exhibited no peeling of the coating surface or significant corrosion even after seven days of immersion. Furthermore, the immersion solution remained clear, indicating a strong bond between the coating and the substrate and significantly improved corrosion resistance compared to the uncoated substrate.

Figure 14 compares the weight loss of the substrate and the sample. As can be seen from this figure, the mass loss of the magnesium alloy substrate increases with the immersion time, and the mass loss increases substantially during the first 48 h of immersion, the mass loss per day within the next 48–96 h is kept in equilibrium, and after 96 h, the mass loss shows an increasing trend. This trend indicates that the corrosion products first generated on the surface are dissolved under the corrosive effect of the chloride medium, and the substrate is further corroded. The samples lost less mass during 0–48 h of immersion, increased substantially at 72 h, and then, contrary to the substrate, the weight lost showed an overall decreasing trend, probably because the structure of the coating surface can deter the penetration of corrosive ions.

The samples soaked for seven days were subjected to electrochemical testing and Fig. 15 shows the polarization curves of the submerged sample compared to the unsoaked sample and substrate. It is evident from the graph that even after 168 h of immersion testing, the corrosion current density of the sample is still less than that of the unsubmerged magnesium alloy substrate.

3.7 Corrosion Behavior and Mechanism

After the anodic reaction (1), magnesium alloys are oxidized to cations, the resulting electrons undergo a reducing cathode reaction (2). Due to the existence of magnesium
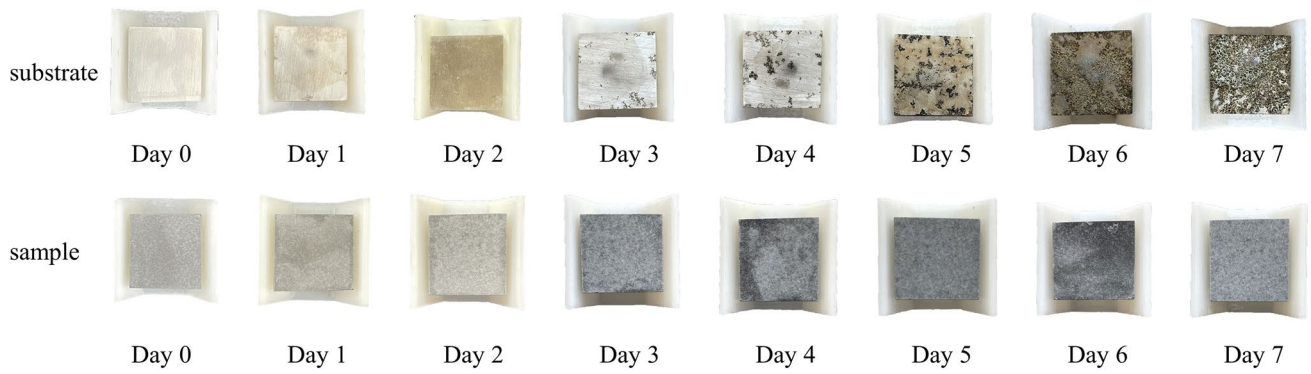
Fig. 13 Morphology variation with immersion time for the uncoated and coated samples in 5 wt% NaCl solution
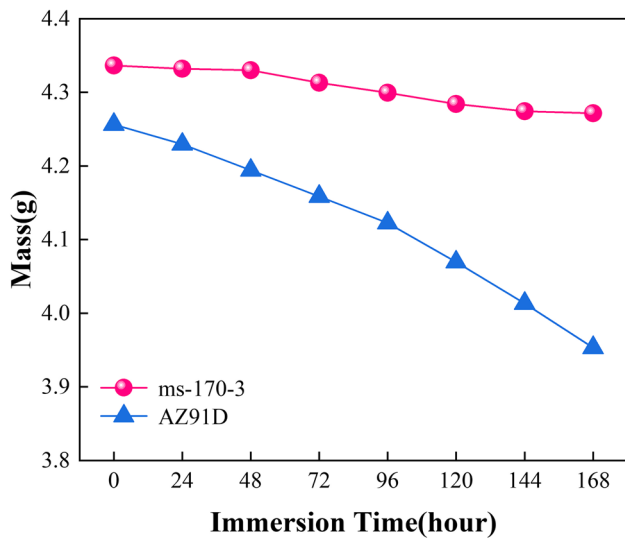

Fig. 14 Mass loss from the substrate and the sample during the immersion test

Fig. 15 Polarization curve of the sample before and after the immersion test

alloy β phase (Mg$_{17}$Al$_{12}$) grain, the Mg-Al microcell is formed between the alloy elements and magnesium. So electrochemical corrosion occurs on the surface of magnesium alloy [50, 51]. Magnesium is also subject to an electrochemical phenomenon known as the negative difference effect (NDE), whereby the corrosion and hydrogen precipitation rates of magnesium increase with increasing potential [52], reaction (3) is the negative differential effect reaction equation for magnesium.
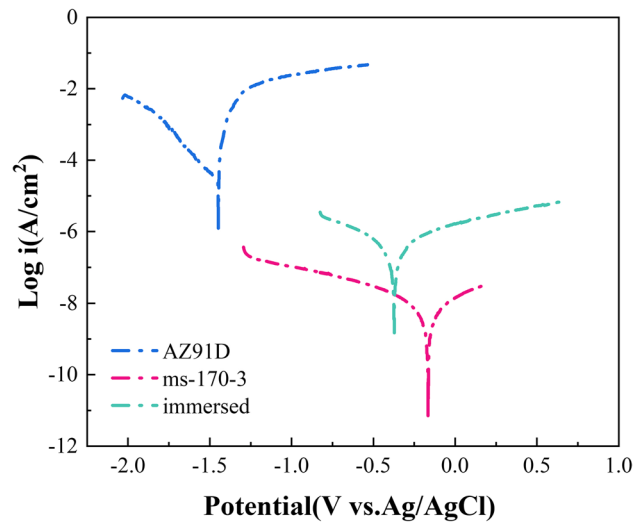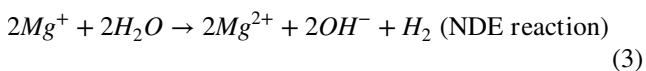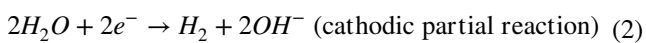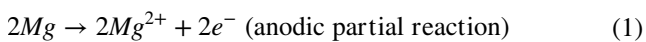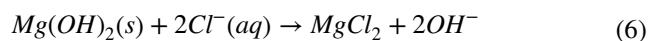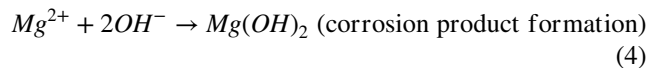
$$2Mg \rightarrow 2Mg^{2+} + 2e^- \text{ (anodic partial reaction)} \quad (1)$$

$$2H_2O + 2e^- \rightarrow H_2 + 2OH^- \text{ (cathodic partial reaction)} \quad (2)$$

$$2Mg^+ + 2H_2O \rightarrow 2Mg^{2+} + 2OH^- + H_2 \text{ (NDE reaction)} \quad (3)$$

$$Mg^{2+} + 2OH^- \rightarrow Mg(OH)_2 \text{ (corrosion product formation)} \quad (4)$$

$$Mg(s) + 2Cl^-(aq) \rightarrow MgCl_2 \quad (5)$$

$$Mg(OH)_2(s) + 2Cl^-(aq) \rightarrow MgCl_2 + 2OH^- \quad (6)$$

When magnesium alloys are subjected to corrosion, they produce the corrosion product magnesium hydroxide (reaction 4), which is slightly soluble in water and slows down the corrosion rate. In sodium chloride solutions, magnesium and magnesium hydroxide react with chloride ions to form highly soluble magnesium chloride (reactions 5 and 6) [47]. As the concentration of MgCl$_2$ produced increases the rate of chemical reaction increases and the rate of corrosion is accelerated. After corrosion, the surfaces of magnesium alloys are more susceptible to anodic and cathodic reactions [53, 54]. The anodic oxidation reaction is a direct reaction

Fig. 16 Dissolution of MMT
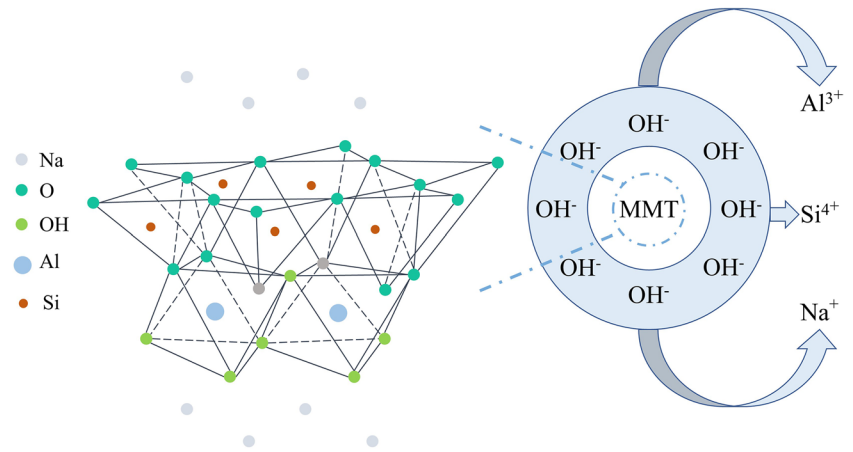
Fig. 17 Dissolution of AZ91D and Silica

$$Mg(OH)_2 \rightleftharpoons Mg^{2+} + 2OH^-$$
$$SiO_2 + 2NaOH \rightarrow Na_2SiO_3 + H_2O$$

Dissolution of AZ91D

Dissolution of silica
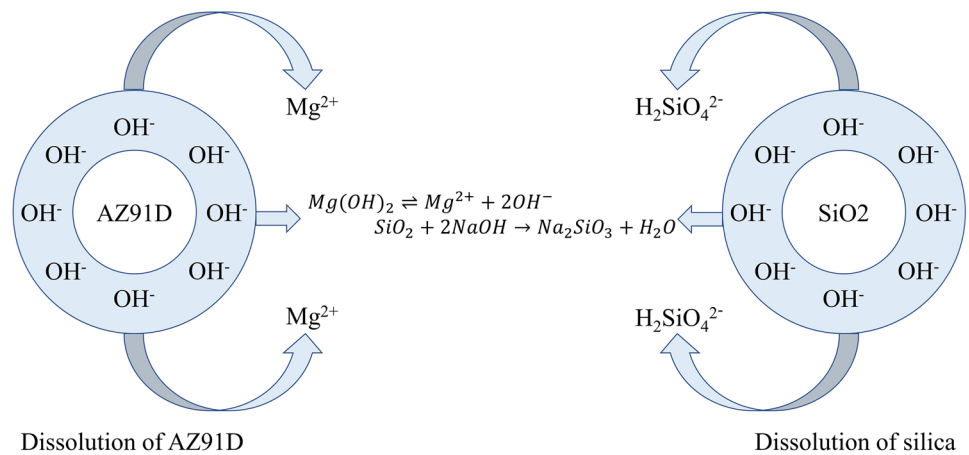
with magnesium hydroxide, where hydroxyl groups reach the surface of the magnesium from the solution through a thin film, thus reducing the corrosion resistance of magnesium alloys [55]. Montmorillonite is difficult to completely dissolve in deionized water due to its water-absorbing and swelling properties, but it can easily dissolve in an alkaline environment as shown in Fig. 16, and the metal cations between the layers are replaced by lower valence cations, providing aluminum and silicon ions for the coating, thus forming a silica-aluminum gel in solution with the silicon ions in the silica, while the excess cations are balanced by OH$^-$ in solution [56].

The multi-layered structure of the composite coating delays the entry of electrolytes from the corrosion solution into the magnesium alloy matrix, delaying the formation of surface corrosion pits and improving the resistance of the magnesium alloy to local pitting [57]. The dissolution of magnesium alloy and silica is shown in Fig. 17.

When silica is added to the solution, the silica film dissolves on the surface of the sample in the form of sodium silicate and adheres tightly to the sample surface to prevent
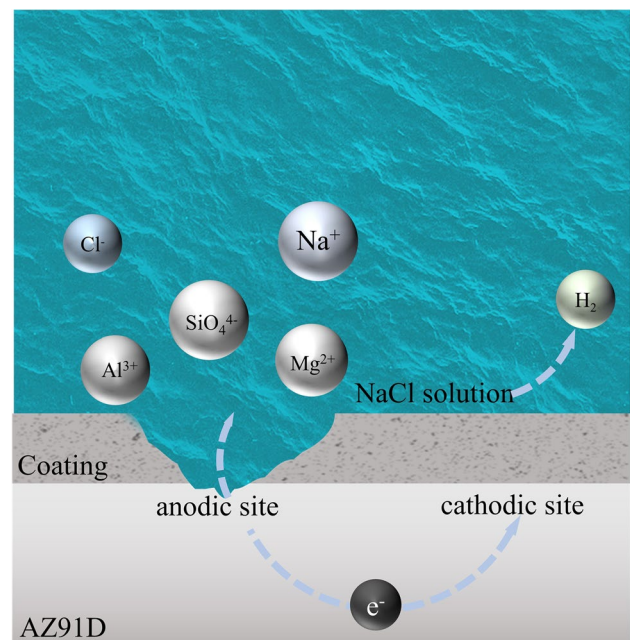
Fig. 18 Corrosion of the sample in NaCl solution

corrosion [58]. The increased polymerization of silicate ions in the solution results in the compacting of the previously loose magnesium hydroxide film and the formation of a dense and homogeneous coating on the surface of the magnesium alloy [59]. Not only does it impede the entry of water molecules, but it also effectively prevents the entry of chloride ions over a large area. As a result, a large amount of chloride ions is located on the outside of the composite coating and only a small amount of chloride ions can pass through the coating [60]. However, when immersed in the solution for a long time, the electrolyte will promote the activation of cracks on the surface of the coating and reduce the adhesion, and the solution will penetrate the metal surface and cause a corrosion reaction, thus reducing the corrosion resistance of the coating [61], The corrosion of the composite coating in solution is shown in Fig. 18.

4 Conclusions

Silicate composite coatings were generated in situ on the surface of a magnesium alloy by a one-step hydrothermal method, and the morphological composition and corrosion resistance mechanism of the coating were investigated using a variety of methods. The following conclusions can be summarized:

1. The reaction time and temperature affected the morphology and properties of the coatings, and sample ms-170-3 had the best corrosion resistance, indicating a four-order of magnitude decrease in corrosion current density compared to AZ91D. It still has corrosion resistance after 168 h of the weight loss test.
2. The composite structure of $Mg(OH)_2$ and silicate on the surface of the coating effectively prevents the entry of electrolyte ions, which improves the corrosion resistance of the magnesium alloy surface.

In summary, the preparation process of the whole experiment is simple, eco-friendly, non-polluting, and the generated composite coating has good protection performance for magnesium alloy substrate and verifies the application of montmorillonite in metal corrosion prevention.

Declarations

This article does not contain any studies with human participants or animals performed by any of the authors.

Consent to Participate Informed consent for publication of this paper was obtained from all authors.

Consent for Publication Informed consent was obtained from all the authors for publication of this report and any accompanying images.

Competing Interests The authors declare no competing interests.

References

1. Heakal FET, Shoeib MA, Maanoum MA (2017) Optimizing parameters affecting Electroless Ni-P Coatings on AZ91D Magnesium Alloy as Corrosion Protection barriers. Prot Met Phys Chem Surf 53(1):177–187
2. Zhao ZY et al (2018) Microstructural evolution and mechanical strengthening mechanism of Mg-3Sn-1Mn-1La alloy after heat treatments. Mater Sci Eng a-Structural Mater Prop Microstruct Process 734:200–209
3. Cui LY et al (2018) In vitro corrosion resistance of a layer-by-layer assembled DNA coating on magnesium alloy. Appl Surf Sci 457:49–58
4. Heakal FET, Bakry AM (2018) Serum albumin can influence magnesium alloy degradation in simulated blood plasma for cardiovascular stenting. Mater Chem Phys 220:35–49
5. Li LY et al (2018) Advances in functionalized polymer coatings on biodegradable magnesium alloys - a review. Acta Biomater 79:23–36
6. Song YW et al (2010) Effect of second phases on the corrosion behavior of wrought Mg-Zn-Y-Zr alloy. Corros Sci 52(5):1830–1837
7. Cui LY et al (2017) Corrosion resistance of a self-healing micro-arc oxidation/polymethyltrimethoxysilane composite coating on magnesium alloy AZ31. Corros Sci 118:84–95
8. Zeng RC et al (2008) Progress and challenge for magnesium alloys as biomaterials. Adv Eng Mater 10(8):B3–B14
9. Thomas S et al (2015) Corrosion mechanism and hydrogen evolution on mg. Curr Opin Solid State Mater Sci 19(2):85–94
10. Ostrowski N et al (2013) Corrosion protection and improved cytocompatibility of biodegradable polymeric layer-by-layer coatings on AZ31 magnesium alloys. Acta Biomater 9(10):8704–8713
11. Oksa M et al (2011) Optimization and characterization of high velocity oxy-fuel sprayed Coatings: techniques, materials, and applications. Coatings 1(1):17–52
12. Abdal-hay A et al (2014) Enhanced biocorrosion resistance of surface modified magnesium alloys using inorganic/organic composite layer for biomedical applications. Ceram Int 40(1):2237–2247
13. Liu WL, Hsieh SH, Chen WJ (2007) Preparation of Sn films deposited on carbon nanotubes. Appl Surf Sci 253(20):8356–8359
14. Kannan MB, Liyanaarachchi S (2013) Hybrid coating on a magnesium alloy for minimizing the localized degradation for load-bearing biodegradable mini-implant applications. Mater Chem Phys 142(1):350–354
15. She ZX et al (2013) Researching the fabrication of anticorrosion superhydrophobic surface on magnesium alloy and its mechanical stability and durability. Chem Eng J 228:415–424
16. Chen J et al (2013) Modifications of the hydrotalcite film on AZ31 mg alloy by phytic acid: the effects on morphology, composition and corrosion resistance. Corros Sci 74:130–138

17. Chen XB et al (2012) Corrosion-resistant electrochemical platings on magnesium alloys: a state-of-the-art review. Corrosion 68(6):518–535

18. Heakal FET, Maanoum MA (2016) Role of some plating parameters in the properties of Ni-P/Al2O3 Nanocomposite Coatings on mg alloy. Int J Electrochem Sci 11(8):7198–7215

19. Lu XY et al (2017) Improvement of protection performance of Mg-rich epoxy coating on AZ91D magnesium alloy by DC anodic oxidation. Prog Org Coat 104:188–198

20. Ivanou DK et al (2013) Plasma anodized ZE41 magnesium alloy sealed with hybrid epoxy-silane coating. Corros Sci 73:300–308

21. Hua L, Sun JP, Wu GS (2022) Enhancing corrosion resistance of hydrothermally-treated magnesium-aluminum alloys by preprocessed metallurgical microstructure. Thin Solid Films 752:139247. https://doi.org/10.1016/j.tsf.2022.139247

22. Calabrese L (2019) Anticorrosion behavior of zeolite coatings obtained by in situ crystallization: a critical review. Materials 12(1):Article 1. https://doi.org/10.3390/ma12010059

23. Bahri H et al (2015) Effect of silica ratio on the corrosion behavior of nano-silica potassium silicate coatings on aluminum alloy 2024. J Mater Eng Perform 24(2):839–847

24. Gu SQ et al (2019) Clay mineral adsorbents for heavy metal removal from wastewater: a review. Environ Chem Lett 17(2):629–654

25. Zhang YJ et al (2013) High corrosion protection of a polyaniline/organophilic montmorillonite coating for magnesium alloys. Prog Org Coat 76(5):804–811

26. Zamanizadeh HR et al (2015) Investigation of the corrosion protection behavior of natural montmorillonite clay/bitumen nanocomposite coatings. Prog Org Coat 78:256–260

27. Jokar M et al (2016) Corrosion and bioactivity evaluation of nanocomposite PCL-forsterite coating applied on 316L stainless steel. Surf Coat Technol 307:324–331

28. Wang J et al (2010) Fabrication of hydrophobic surface with hierarchical structure on mg alloy and its corrosion resistance. Electrochim Acta 55(22):6897–6906

29. Zhu JY, Jia CX (2022) Preparation of corrosion-resistant hydrophobic composite films on magnesium alloy. Surf Eng 38(7–9):713–724

30. Li WD (2022) Effects of ca and ag addition and heat treatment on the corrosion behavior of Mg-7Sn alloys in 3.5 wt.% NaCl solution. Surf Interface Anal 54(6):631–641

31. Zhu JY, Jia CX, Duan YZ (2023) Study on corrosion resistance of alkali-heat modified magnesium alloy surface. Met Mater Int 29(6):1638–1651

32. Yang CW et al (2017) Hydrothermal treatment and butylphosphonic acid derived self-assembled monolayers for improving the surface chemistry and corrosion resistance of AZ61 magnesium alloy. Sci Rep 7(1):Article 1. https://doi.org/10.1038/s41598-017-17199-z

33. Jeong H, Yoo Y (2015) Synthesis and characterization of thin films on magnesium alloy using a hydrothermal method. Surf Coat Technol 284:26–30

34. Morgan WE, Wazer JRV, Stec WJ (1973) Inner-orbital photoelectron spectroscopy of the alkali metal halides, perchlorates, phosphates, and pyrophosphate. J Am Chem Soc 95(3):751–755

35. Thomas TD et al (1986) Valence electronic structure of AuZn and AuMg alloys derived from a new way of analyzing Auger-parameter shifts. Phys Rev B 33(8):5406–5413. https://doi.org/10.1103/physrevb.33.5406

36. Della Rovere CA et al (2012) Characterization of passive films on shape memory stainless steels. Corros Sci 57:154–161

37. Robin R, Miserque F, Spagnol V (2008) Correlation between composition of passive layer and corrosion behavior of high Si-containing austenitic stainless steels in nitric acid. J Nucl Mater 375(1):65–71

38. Okada K, Kameshima Y, Yasumori A (1998) Chemical shifts of silicon X-ray photoelectron spectra by polymerization structures of silicates. J Am Ceram Soc 81(7):1970–1972

39. Li J et al (2016) Facile fabrication of superhydrophobic silica coatings with excellent corrosion resistance and liquid marbles. J Solgel Sci Technol 80(1):208–214

40. Heakal FE et al (2012) Investigation on the corrosion and hydrogen evolution for AZ91D magnesium alloy in single and anion-containing oxalate solutions. Int J Hydrog Energy 37(1):84–94

41. Tian HL, Su Z, Zhang YH (2017) Synthesis and electrochemical properties of spinel LiCrTiO4 and its application in LiFePO4/LiCrTiO4 full cells. Int J Electrochem Sci 12(8):6980–6989

42. Wang B et al (2022) Study on anti-corrosion performance of silica fume modified magnesium potassium phosphate cement-based coating on steel. Case Stud Constr Mater 17:e01467. https://doi.org/10.1016/j.cscm.2022.e01467

43. Amrollahi S et al (2019) Synthesis of polyaniline-modified graphene oxide for obtaining a high performance epoxy nanocomposite film with excellent UV blocking/anti-oxidant/anti-corrosion capabilities. Compos Part B-Eng 173:106804. https://doi.org/10.1016/j.compositesb.2019.05.015

44. Heakal FET, Fekry AM, Fatayerji MZ (2009) Influence of halides on the dissolution and passivation behavior of AZ91D magnesium alloy in aqueous solutions. Electrochim Acta 54(5):1545–1557

45. Diaz-Ramos M et al (2023) Electrochemical Impedance Spectroscopy (EIS) of parylene coated magnesium stents in organic solvent to study early corrosion control. Corros Sci 213:110932. https://doi.org/10.1016/j.corsci.2022.110932

46. Zhao DW et al (2017) Current status on clinical applications of magnesium-based orthopaedic implants: a review from clinical translational perspective. Biomaterials 112:287–302

47. Esen Z, Butev E, Karakas MS (2016) A comparative study on biodegradation and mechanical properties of pressureless infiltrated Ti/Ti6Al4V-Mg composites. J Mech Behav Biomed Mater 63:273–286

48. Wang FS et al (2020) A method to select the optimal equivalent electrical circuit applied to study corrosion system of composite coating on magnesium alloy. Phys Lett A 384(24):126452. https://doi.org/10.1016/j.physleta.2020.126452

49. Zeng LY et al (2010) Preparation and characterization of a double-layer coating on magnesium alloy AZ91D. Electrochim Acta 55(9):3376–3383

50. Heakal FE, Shehata OS, Tantawy NS (2014) Degradation behaviour of AZ80E magnesium alloy exposed to phosphate buffer saline medium. Corros Sci 86:285–294

51. Liu LJ, Schlesinger M (2009) Corrosion of magnesium and its alloys. Corros Sci 51(8):1733–1737

52. Bender S et al (2012) A new theory for the negative difference effect in magnesium corrosion. Mater Corrosion-Werkstoffe Und Korrosion 63(8):707–712

53. Baril G et al (2007) An impedance investigation of the mechanism of pure magnesium corrosion in sodium sulfate solutions. J Electrochem Soc 154(2):C108–C113

54. Heakal FET et al (2022) Influence of anodization and bovine serum albumin on the degradation of new AXJ-magnesium alloy system as a bioabsorbable orthopedic implant. J Electroanal Chem 918:116458. https://doi.org/10.1016/j.jelechem.2022.116458

55. Cai ZP et al (2009) Study on anodic oxidation of magnesium in 6 M KOH solution by alternative current impedance. Int J Hydrog Energy 34(1):467–472

56. Zhu TT et al (2019) Exfoliation of montmorillonite and related properties of clay/polymer nanocomposites. Appl Clay Sci 169:48–66

57. Hayajneh MT, Almomani MA, Al HB, Hmoud (2019) Corrosion evaluation of nanocomposite gelatin-forsterite coating applied on AISI 316L stainless steel. Mater Res Express 6(11):116431. https://doi.org/10.1088/2053-1591/ab49c3

58. Li CB et al (2021) Study on the synergistic corrosion inhibition effect between Sodium Silicate and Triethanolamine for 45 Steel Corrosion in 3.5% NaCl solution. Int J Electrochem Sci 16(10):211034. https://doi.org/10.20964/2021.10.59

59. Jamali F, Danaee I, Zaarei D (2015) Effect of nano-silica on the corrosion behavior of silicate conversion coatings on hot-dip galvanized steel. Mater Corrosion-Werkstoffe Und Korrosion 66(5):459–464

60. Yu LT et al (2022) Simultaneously improving the mechanical property and corrosion resistance of extruded biomedical Mg-3Zn alloy by forming in-situ MgO. J Mater Res Technol-Jmr&T 18: 2977–2992

61. Calabrese L et al (2014) Electrochemical behavior of hydrophobic silane-zeolite coatings for corrosion protection of aluminum substrate. J Coat Technol Res 11(6):883–898